Unifying quantum heat transfer in a nonequilibrium spin-boson model with full counting statistics

Chen Wang,[1,*] Jie Ren,[2,3,4,†] and Jianshu Cao[5,‡]

[1]*Department of Physics, Hangzhou Dianzi University, Hangzhou, Zhejiang 310018, People's Republic of China*

[2]*Center for Phononics and Thermal Energy Science, School of Physics Science and Engineering, Tongji University, 200092 Shanghai, People's Republic of China*

[3]*China-EU Joint Center for Nanophononics, School of Physics Science and Engineering, Tongji University, 200092 Shanghai, People's Republic of China*

[4]*Shanghai Key Laboratory of Special Artificial Microstructure Materials and Technology, School of Physics Science and Engineering, Tongji University, 200092 Shanghai, People's Republic of China*

[5]*Department of Chemistry, Massachusetts Institute of Technology, 77 Massachusetts Avenue, Cambridge, Massachusetts 02139, USA*

(Received 12 December 2016; revised manuscript received 8 January 2017; published 13 February 2017)

To study the full counting statistics of quantum heat transfer in a driven nonequilibrium spin-boson model, we develop a generalized nonequilibrium polaron-transformed Redfield equation with an auxiliary counting field. This enables us to study the impact of qubit-bath coupling ranging from weak to strong regimes. Without external modulations, we observe maximal values of both steady-state heat flux and noise power in moderate coupling regimes, below which we find that these two transport quantities are enhanced by the finite-qubit-energy bias. With external modulations, the geometric-phase-induced heat flux shows a monotonic decrease upon increasing the qubit-bath coupling at zero qubit energy bias (without bias). While under the finite-qubit-energy bias (with bias), the geometric-phase-induced heat flux exhibits an interesting reversal behavior in the strong coupling regime. Our results unify the seemingly contradictory results in weak and strong qubit-bath coupling regimes and provide detailed dissections for the quantum fluctuation of nonequilibrium heat transfer.

DOI: 10.1103/PhysRevA.95.023610

I. INTRODUCTION

Efficient realization and smart control of quantum energy transfer are of fundamental importance in various fields, ranging from molecular electronics, to quantum heat engine, to quantum biology [1–5]. In particular, information and heat flow have been extensively studied in thermal functional devices, spawning phononics [6,7], where phonons are flexibly manipulated in analogy with electronic current in modern electronics [8–13]. In accordance with the second law of thermodynamics, it is known that heat energy will naturally transfer from a hot source to a cold drain driven by the thermodynamic bias (e.g., temperature), without an external driving field. Considering external modulations, the optimal mechanism of dynamical control can be unraveled in phononic thermal systems [14–17], even to pump heat against the temperature bias.

The prototype for describing nanoscale heat transfer mediated by quantum junctions is the nonequilibrium spin-boson (NESB) model [8,18], which was originally proposed in the study of quantum dissipation [19,20]. The NESB model is composed of a two-level system (i.e., qubit) interacting with two bosonic thermal baths under temperature bias. Many methods have been proposed to study the microscopic mechanism of quantum heat transfer in the NESB model. Particularly, the Redfield approach has been extensively applied to analyze the weak qubit-bath coupling regime, mainly due to the effective expression and clear physical picture [14,15]. The contribution of two thermal baths to the heat flux is additive, which means that only incoherently sequential heat-exchange processes between the qubit and baths are considered. As such, the limitation of the Redfield approach is exposed in the strong qubit-bath coupling regime, where the heat flux is nonlinearly dependent on the system-bath coupling strength. In sharp contrast, the nonequilibrium nonteracting-blip approximation (NIBA) is applicable in the strong coupling limit to analytically treat multiphonon processes [9,21–23], where nonadditive and cooperative phonon transfer processes are included. Particularly, the appearance of turnover behavior of heat flux as a function of the qubit-bath coupling strength in the NESB model was confirmed by the NIBA, as well as by the multilayer multiconfiguration Hartree [24], quantum Monte Carlo schemes [18], and the nonequilibrium Green's function method [25–27]. Recently, the nonequilibrium polaron-transformed Redfield equation (NE-PTRE) has been proposed by the authors to analytically unify the steady-state heat flux in the weak and strong coupling limits, and the parity classified transfer processes have been unraveled [28].

From the dynamical control perspective, the time-dependent modulation of heat transfer in the NESB model has also attracted tremendous attention, enriching the transfer mechanisms [14–17,29–33]. The typical realization of the dynamical modulation is the adiabatic quantum pump, which was originally proposed by D. J. Thouless to study the effect of Berry-phase-induced quantization on closed-system transport [34]. In analogy, as the NESB model is adiabatically and periodically driven by control parameters (e.g., bath temperatures), a geometric-phase-induced heat flow will contribute to the heat transfer [15,16]. However, previous research unraveled the seemingly contradictory results that, in the weak qubit-bath coupling limit, the geometric-phase-induced heat flux remains finite, independent of the qubit-bath coupling strength under the unbiased condition [15], whereas

*wangchenyifang@gmail.com
†Xonics@tongji.edu.cn
‡jianshu@mit.edu

the counterpart in the strong coupling limit becomes strictly 0 [16]. The statement of seemingly contradiction or seemingly contradictory results below has the same meaning as expressed herein by default. Thus, natural questions are raised: What happens in the intermediate qubit-bath coupling regime? and Can we propose a theory to unify the geometric-phase-induced heat flux in the weak and strong coupling limits?

In the present paper, by including the full counting statistics, we introduce a generalized NE-PTRE to analyze the geometric-phase-induced heat flux in the NESB model. Our NE-PTRE is able to accommodate both the sequential transfer picture in the weak coupling limit and the multiphonon involved nonlinear collective transfer picture in the strong coupling regime. The geometric heat pump is investigated under both unbiased and biased conditions, and the seemingly contradictory results in the weak and strong coupling limits are clearly unified. Moreover, the effect of the qubit energy bias on the geometric heat pump is analyzed in typical system-bath coupling regimes. This work is organized as follows: in Sec. II, we introduce the NESB model and the NE-PTRE scheme that dissect the phonon transfer details. Then in Sec. III, by introducing the full counting statistics, we develop the generalized NE-PTRE and systematically analyze the counting measurements of NESB transport. In Sec. IV, first we investigate the steady-state heat flux and noise power as functions of the coupling strength and qubit energy bias. Then we focus on the geometric-phase-induced heat flux in both the unbiased and the biased cases, and comparisons with Redfield and nonequilibrium NIBA are clearly demonstrated. The final section (Sec. V) provides a concise summary.

II. NONEQUILIBRIUM SPIN-BOSON SYSTEM

A. Model

Following Ref. [28], the NESB model in Fig. 1, consisting of a two-level qubit coupled to two phononic thermal baths at different temperatures [8,15,18–20], is described as

$$\hat{H}_0 = \frac{\epsilon_0}{2}\hat{\sigma}_z + \frac{\Delta}{2}\hat{\sigma}_x + \sum_{k;v=L,R}\omega_k \hat{b}^\dagger_{k,v}\hat{b}_{k,v} + \sum_{k;v=L,R}\hat{\sigma}_z(\lambda_{k,v}\hat{b}^\dagger_{k,v} + \lambda^*_{k,v}\hat{b}_{k,v}), \quad (1)$$

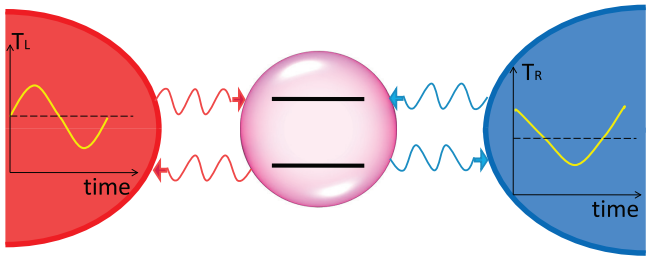

FIG. 1. Schematic of the nonequilibrium spin-boson model, composed of a central two-level qubit (purple circle) coupled to two individual thermal baths (red and blue regions), with temperatures T_L and T_R, respectively. Wavy red (blue) arrowed lines describe the interaction between the qubit and the Lth (Rth) bath. For the driven nonequilibrium spin-boson model, the system parameters appear to be time dependent, e.g., $T_L(t)$ and $T_R(t)$.

where the qubit is specified by the Pauli operators $\hat{\sigma}_z = |1\rangle\langle 1| - |0\rangle\langle 0|$ and $\hat{\sigma}_x = |1\rangle\langle 0| + |0\rangle\langle 1|$, with $|1(0)\rangle$ the excited (ground) state. ϵ_0 is the energy bias, and Δ is the tunneling strength between two states. $\hat{b}^\dagger_{k,v}$ ($\hat{b}_{k,v}$) creates (annihilates) one phonon with energy ω_k and momentum k in the vth bath, and $\lambda_{k,v}$ describes the coupling strength between the qubit and the vth bath.

To study the qubit-bath interaction beyond the weak coupling limit, it is helpful to transform the original Hamiltonian $\hat{H}_0$ in Eq. (1) under the polaron framework by $\hat{H} = \hat{U}^\dagger\hat{H}_0\hat{U}$ [9,16,35], where the unitary operator is given by $\hat{U} = e^{i\hat{\sigma}_z\hat{B}/2}$, with the collective phononic momentum operator $\hat{B} = 2i\sum_{k;v=L,R}(\frac{\lambda_{k,v}}{\omega_k}\hat{b}^\dagger_{k,v} - \frac{\lambda^*_{k,v}}{\omega_k}\hat{b}_{k,v})$. Thus, the transformed Hamiltonian becomes $\hat{H} = \hat{H}_s + \hat{H}_b + \hat{V}_{sb}$. Specifically, the reorganized two-level qubit is shown as

$$\hat{H}_s = \frac{\epsilon_0}{2}\hat{\sigma}_z + \frac{\eta\Delta}{2}\hat{\sigma}_x, \quad (2)$$

where the renormalization factor is given by [9,16]

$$\eta = \langle\cos\hat{B}\rangle = \exp\left(-\sum_v\int_0^\infty d\omega\frac{J_v(\omega)}{\pi\omega^2}[n_v(\omega)+1/2]\right), \quad (3)$$

with the vth bath spectral function $J_v(\omega) = 4\pi\sum_k|\lambda_{k,v}|^2\delta(\omega-\omega_k)$, the Bose-Einstein distribution $n_v(\omega) = 1/[\exp(\beta_v\omega_v)-1]$, and the inverse of the vth bath temperature $\beta_v = 1/k_BT_v$. The noninteracting phonon baths are characterized as $\hat{H}_b = \sum_{v=L,R}\hat{H}_v$, with $\hat{H}_v = \sum_k\omega_k\hat{b}^\dagger_{k,v}\hat{b}_{k,v}$. The qubit-bath interaction is expressed as

$$\hat{V}_{sb} = \frac{\Delta}{2}[(\cos\hat{B}-\eta)\hat{\sigma}_x + \sin\hat{B}\hat{\sigma}_y], \quad (4)$$

of which the thermal average vanishes, i.e., $\langle\hat{V}_{sb}\rangle = 0$. Hence, it may be appropriate to perturbatively obtain the equation of motion for the two-level qubit in the polaron picture. It should be noted that in many traditional approaches including many-phonon processes, e.g., the NIBA, the system-bath interaction $\hat{V} = \frac{\Delta}{2}(\cos\hat{B}\hat{\sigma}_x + \sin\hat{B}\hat{\sigma}_y)$ is directly perturbed [9,16]. However, actually $\hat{V}$ should not be treated as a perturbation due to the nonnegligible contribution of $\langle\hat{V}\rangle \neq 0$. In contrast, $\hat{V}_{sb} = \hat{V} - \langle\hat{V}\rangle$ in Eq. (4) may be properly perturbed in accordance with the perturbation theory [28].

In this paper, the spectral function of phonon baths is characterized as $J_v(\omega) = \pi\alpha_v\omega^s\omega_{c,v}^{1-s}e^{-\omega/\omega_{c,v}}$, which is typically considered in quantum transfer studies of nanojunction systems [20,35–39]. α_v is the system-bath coupling strength of the order $\alpha_v \sim |\lambda_{k,v}|^2$, and $\omega_{c,v}$ is the cutoff frequency of the vth phonon bath. Without loss of generality, we consider the superohmic spectrum $s = 3$ in this study. Hence, the renormalization factor is specified as $\eta = \exp\{-\sum_{v=L,R}\alpha_v[-1 + \frac{2}{(\beta_v\omega_{c,v})^2}\psi_1(1/\beta_v\omega_{c,v})]/2\}$, with the trigamma function $\psi_1(x) = \sum_{n=0}^\infty\frac{1}{(n+x)^2}$. Moreover, in the weak coupling limit $\alpha_v \ll 1$, the normalization factor η becomes 1, while in the strong coupling regime $\alpha_v \gg 1$, it vanishes ($\eta = 0$).

B. Nonequilibrium polaron-transformed Redfield equation

We note that the PTRE method was originally developed to study quantum dissipative dynamics [35–38,40], with a single bath. Here we handle a system coupled to at least two baths at nonequilibrium. It is known that the reorganized system-bath interaction $\hat{V}_{sb}$ can be treated as a perturbation [28]. Based on the Born-Markov approximation and the second-order perturbation theory, we obtain the NE-PTRE as

$$\frac{\partial\hat{\rho}}{\partial t} = -i[\hat{H}_s,\hat{\rho}] + \sum_{l=e,o}\sum_{\omega,\omega'=0,\pm\Lambda}\Gamma_l(\omega)[\hat{P}_l(\omega)\hat{\rho},\hat{P}_l(\omega')] + \text{H.c.}, \tag{5}$$

where $\hat{\rho}$ is the reduced density matrix of the qubit in the polaron picture, $\Lambda=\sqrt{\epsilon_0^2+\eta^2\Delta^2}$ is the energy gap in the eigenbasis, and $\hat{P}_{e(o)}(\omega)$ is the eigenstate transition projector (see [41]), of which the relation to Pauli matrices is given by $\hat{\sigma}_{x(y)}(-\tau)=\sum_{\omega=0,\pm\Lambda}\hat{P}_{e(o)}(\omega)e^{i\omega\tau}$. The transition rates are

$$\Gamma_o(\omega) = \left(\frac{\eta\Delta}{2}\right)^2\int_0^\infty d\tau e^{i\omega\tau}\sum_{n=0}^{\infty}\frac{Q(\tau)^{2n+1}}{(2n+1)!}, \tag{6}$$

$$\Gamma_e(\omega) = \left(\frac{\eta\Delta}{2}\right)^2\int_0^\infty d\tau e^{i\omega\tau}\sum_{n=1}^{\infty}\frac{Q(\tau)^{2n}}{(2n)!}, \tag{7}$$

with the collective phonon propagator $Q(\tau)=\sum_{v=L,R}Q_v(\tau)$, and

$$Q_v(\tau) = \int_0^\infty d\omega\frac{J_v(\omega)}{\pi\omega^2}\{n_v(\omega)e^{i\omega\tau}+[1+n_v(\omega)]e^{-i\omega\tau}\}. \tag{8}$$

From expressions of the correlation functions $\Gamma_{e(0)}(\omega)$, it is clearly shown that phonon transfer processes are classified by the even- and odd-parity contributions. Specifically, $\Gamma_o(\tau)$ describes the transfer processes including odd phonon numbers from two baths. The lowest order term $\Gamma_o^{(1)}(\omega)$ contains the terms $\frac{(\eta\Delta)^2}{8}[Q_L(\omega)+Q_R(\omega)]$, with the individual bath contribution $Q_v(\omega)=\int_{-\infty}^{\infty}d\tau e^{i\omega\tau}Q_v(\tau)$ at the transition energy $\omega=\pm\Lambda$, so that the lowest odd parity exhibits sequential-tunneling behavior depicted in Figs. 2(a) and 2(b) [8,15] while $\Gamma_e(\omega)$ shows cooperative heat transfer processes involving even phonon numbers. The corresponding lowest order even term $\Gamma_e^{(1)}(0)$ describes the cotunneling effect at Figs. 2(c) and 2(d) [42], which contains $\frac{(\eta\Delta)^2}{8\pi}\int_{-\infty}^{\infty}d\omega Q_L(\omega)Q_R(-\omega)=\frac{(\eta\Delta)^2}{8\pi}\int_0^\infty d\omega[Q_L(\omega)Q_R(-\omega)+Q_R(\omega)Q_L(-\omega)]$. This demonstrates the physical picture that as the left bath releases thermal energy ω, the right bath gains the equivalent quanta simultaneously, and the two-level system only has the virtual processes of excitation and relaxation so that it remains intact. Apparently, these contributions from two baths are involved nonadditively. Moreover, we can obtain an arbitrary order contribution to heat transfer processes systematically by applying the Taylor expansion.

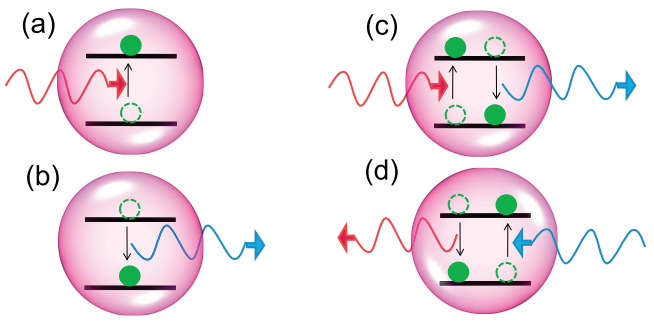

FIG. 2. Representative processes involving phonons in quantum heat transfer: (a), (b) single-phonon sequentially incoherent processes, $Q_L(\omega)$ and $Q_R(-\omega)$, respectively; (c), (d) two-phonon cotunneling processes, $Q_L(\omega)Q_R(-\omega)$ and $Q_R(\omega)Q_L(-\omega)$, respectively.

Particularly, without bias ($\epsilon_0=0$) the steady-state densities can be obtained analytically in the local basis, where the diagonal and off-diagonal terms are [28]

$$P_{11} = P_{00} = 1/2, \tag{9}$$

$$P_{10} = P_{01} = \frac{1}{2}\frac{\text{Re}[\Gamma_o(-\Lambda)]-\text{Re}[\Gamma_o(\Lambda)]}{\text{Re}[\Gamma_o(-\Lambda)]+\text{Re}[\Gamma_o(\Lambda)]}, \tag{10}$$

with the element $P_{ij}=\lim_{t\to\infty}\langle i|\hat{\rho}(t)|j\rangle$ ($|i\rangle$ depicts the qubit state), energy gap $\Lambda=\eta\Delta$, and $\text{Re}[\Gamma_{o(e)}(\omega)]$ the real part of $\Gamma_{o(e)}(\omega)$.

III. FULL COUNTING STATISTICS OF THE NESB MODEL

We study the statistics of the transported heat $\Delta q_\tau=\sum_k\omega_k\Delta n_{k,v}$ in the NESB model, from the system to the vth phonon bath during a time interval τ, with $\Delta n_{k,v}$ the change in phonon number to the initial one with momentum k. The specific measurement of Δq_τ can be conducted as follows: Initially at time $t=0$, we introduce a projector $\hat{K}_{q_0}=|q_0\rangle\langle q_0|$ to measure the quantity $\hat{H}_v=\sum_k\omega_k\hat{b}_{k,v}^\dagger\hat{b}_{k,v}$ in the vth bath, giving $q_0=\sum_k\omega_k n_{k,v}(0)$. After a finite time τ of evolution of the system coupled to thermal baths, we again perform the projection $\hat{K}_{q_\tau}=|q_\tau\rangle\langle q_\tau|$ to obtain the measurement outcome $q_\tau=\sum_k\omega_k n_{k,v}(\tau)$. Hence, the number difference is given by $\Delta n_{k,v}=n_{k,v}(\tau)-n_{k,v}(0)$. Meanwhile, the joint probability of measuring q_0 at $t=0$ and q_τ at $t=\tau$ is defined as [43]

$$\text{Pr}[q_\tau,q_0] = \text{Tr}_{s,b}\{\hat{K}_{q_\tau}e^{-i\hat{H}_0\tau}\hat{K}_{q_0}\hat{\rho}_0\hat{K}_{q_0}e^{i\hat{H}_0\tau}\hat{K}_{q_\tau}\}, \tag{11}$$

with the trace over both the qubit and the thermal baths. Based on the joint probability $\text{Pr}[q_\tau,q_0]$, we introduce the probability of measuring Δq_τ during the time interval τ as

$$\text{Pr}_\tau(\Delta q_\tau) = \sum_{q_\tau,q_0}\delta(\Delta q_\tau-(q_\tau-q_0))\text{Pr}[q_\tau,q_0]. \tag{12}$$

Then the cumulant generating function of the statistics can be defined as

$$G_\tau(\chi) = \ln\int d\Delta q_\tau\text{Pr}_\tau(\Delta q_\tau)e^{i\chi\Delta q_\tau}, \tag{13}$$

with χ the counting-field parameter.

To quantitatively express the cumulant generating function, we introduce the NE-PTRE accompanied by the full counting statistics. Assuming that the quantum system is connected to two baths (labeled L and R), we measure the transported heat from the system to the Rth bath, in the context of the χ-dependent NE-PTRE. Then we add the counting projector

to the Hamiltonian $\hat{H}_0$ in Eq. (1) to generate $\hat{H}_0(\chi) = e^{i\chi\hat{H}_R/2}\hat{H}_0 e^{i\chi\hat{H}_R/2}$ [43,44], written as

$$\hat{H}_0(\chi) = \frac{\epsilon_0}{2}\hat{\sigma}_z + \frac{\Delta}{2}\hat{\sigma}_x + \sum_{k;v=L,R}\omega_k \hat{b}^\dagger_{k,v}\hat{b}_{k,v} + \sum_{k;v=L,R}\hat{\sigma}_z(e^{i\chi\omega_k\delta_{v,R}/2}\lambda_{k,v}\hat{b}^\dagger_{k,v} + \text{H.c.}). \quad (14)$$

Similarly to the transformation scheme in the NE-PTRE [28], we perform a generalized polaron transformation resulting in $\hat{H}_\chi = \hat{U}^\dagger_\chi \hat{H}_0(\chi)\hat{U}_\chi$, with the unitary operator $U_\chi = e^{i\hat{\sigma}_z\hat{B}_\chi/2}$ and χ-dependent phonon collective momentum $\hat{B}_\chi = 2i\sum_{k,v}(e^{i\chi\omega_k\delta_{v,R}/2}\frac{\lambda_{k,v}}{\omega_k}\hat{b}^\dagger_{k,v} - \text{H.c.})$. As such, the transformed Hamiltonian is expressed as $\hat{H}_\chi = \hat{H}_s + \hat{H}_b + \hat{V}_{sb}(\chi)$. Particularly, the reorganized qubit-bath coupling is modified by the counting field as

$$\hat{V}_{sb}(\chi) = \frac{\Delta}{2}[(\cos\hat{B}_\chi - \eta)\hat{\sigma}_x + \sin\hat{B}_\chi\hat{\sigma}_y], \quad (15)$$

which includes both the information on the counting measurement and the multiphonon nonlinear processes. Whereas $\hat{H}_s$ and $\hat{H}_b$ remain unchanged, it should be noted that the thermal average of the interaction term vanishes $\langle\hat{V}_{sb}(\chi)\rangle = 0$ due to the parity symmetry. Moreover, the magnitude of the second-order correlated contribution of $\hat{V}_{sb}(\chi)$ is quite small, compared to $\hat{H}_s$ at Eq. (2). Hence, the perturbation of $\hat{V}_{sb}(\chi)$ can be properly carried out, like the derivation of Eq. (5). Considering the Born-Markov approximation, we perturb $\hat{V}_{sb}(\chi)$ up to second order and obtain the generalized NE-PTRE in the context of full counting statistics,

$$\frac{\partial\hat{\rho}_\chi}{\partial t} = -i[\hat{H}_s,\hat{\rho}_\chi] + \sum_{l=e,0}\sum_{\omega,\omega'=0,\pm\Lambda}\{[\Gamma^\chi_{l,-}(\omega) + \Gamma^\chi_{l,+}(\omega')] \times \hat{P}_l(\omega')\hat{\rho}_\chi\hat{P}_l(\omega) - [\Gamma_{l,+}(\omega)\hat{P}_l(\omega')\hat{P}_l(\omega)\hat{\rho}_\chi + \text{H.c.}]\}, \quad (16)$$

where $\hat{\rho}_\chi$ is the reduced two-level system (qubit) density operator under the counting field, $\hat{P}_l(\omega)$ is the eigenstate transition projector [41], and the energy gap is $\Lambda = \sqrt{\epsilon_0^2 + \eta^2\Delta^2}$. The transition rates are expressed as

$$\Gamma^\chi_{e,\sigma}(\omega) = \left(\frac{\eta\Delta}{2}\right)^2\int_0^\infty d\tau e^{i\omega\tau}[\cosh Q(\sigma\tau - \chi) - 1], \quad (17)$$

$$\Gamma^\chi_{o,\sigma}(\omega) = \left(\frac{\eta\Delta}{2}\right)^2\int_0^\infty d\tau e^{i\omega\tau}\sinh Q(\sigma\tau - \chi), \quad (18)$$

where the modified single-phonon propagator becomes $Q(\tau - \chi) = Q_L(\tau) + Q_R(\tau - \chi)$.

IV. RESULTS AND DISCUSSION

In this section, we apply the generalized nonequilibrium polaron-transformed Redfield equation with an auxiliary counting field, to study the steady-state heat transfer, as well as the geometric-phase-induced heat transfer under adiabatic time-dependent modulations.

A. Steady-state heat transfer

By rearranging the NE-PTRE in the Liouville space [28], the equation of motion for the two-level qubit in Eq. (16) is expressed as

$$\frac{\partial}{\partial t}|\rho_\chi\rangle = -\hat{\mathcal{L}}_\chi|\rho_\chi\rangle, \quad (19)$$

where the vector form of the density matrix is $|\rho_\chi\rangle = [P^\chi_{11}, P^\chi_{00}, P^\chi_{10}, P^\chi_{01}]^T$ with $P^\chi_{ij} = \langle i|\hat{\rho}_\chi|j\rangle$, and $\hat{\mathcal{L}}_\chi$ is the Liouvillion superoperator. In the absence of the counting-field parameter ($\chi = 0$), the element of the density operator P^χ_{ij} reduces to the conventional P_{ij}. Based on the dynamical equation, (19), the reduced density matrix at time t is given by $|\rho_\chi(t)\rangle = \exp(-\hat{\mathcal{L}}_\chi t)|\rho_\chi(0)\rangle$, with $|\rho_\chi(0)\rangle$ the initial state. Hence, the cumulant function can be expressed as $\mathcal{Z}_\chi(t) = \langle\text{I}|\rho_\chi(t)\rangle$ [44], with the unit vector defined as $\langle\text{I}| = [1,1,0,0]$. Consequently, the cumulant generating function after long-time evolution can be obtained by $G_t(\chi) = \frac{1}{t}\ln\mathcal{Z}_\chi(t)$, and the corresponding nth cumulant of heat current fluctuations can be generated as $J^{(n)}(t) = \langle\hat{Q}^n\rangle/t = \frac{\partial^n G_t(\chi)}{\partial(i\chi)^n}|_{\chi=0}$. When external modulation is absent, i.e., $\mathcal{L}_\chi$ is time independent, if we focus on the steady-state solution, the cumulant generating function is simplified to $G(\chi) = -E_0(\chi)$, where $E_0(\chi)$ is the ground-state energy of the superoperator $\hat{\mathcal{L}}_\chi$. The corresponding left and right eigenvectors are denoted $\langle\Phi_\chi|$ and $|\Psi_\chi\rangle$, which fulfill the normalization relation $\langle\Phi_\chi|\Psi_\chi\rangle = 1$. In particular, the steady-state heat flux is the first cumulant $J = -\frac{\partial E_0(\chi)}{\partial(i\chi)}|_{\chi=0}$, and the noise power is the second cumulant $J^{(2)} = -\frac{\partial^2 E_0(\chi)}{\partial(i\chi)^2}|_{\chi=0}$.

1. *Unbiased condition:* $\epsilon_0 = 0$

We first investigate the steady-state heat transfer in Fig. 3, where the system parameters are time independent. Without bias ($\epsilon_0 = 0$), the authors have shown in Ref. [28] that the heat flux can be analytically solved over a wide system-bath coupling regime by applying the NE-PTRE.

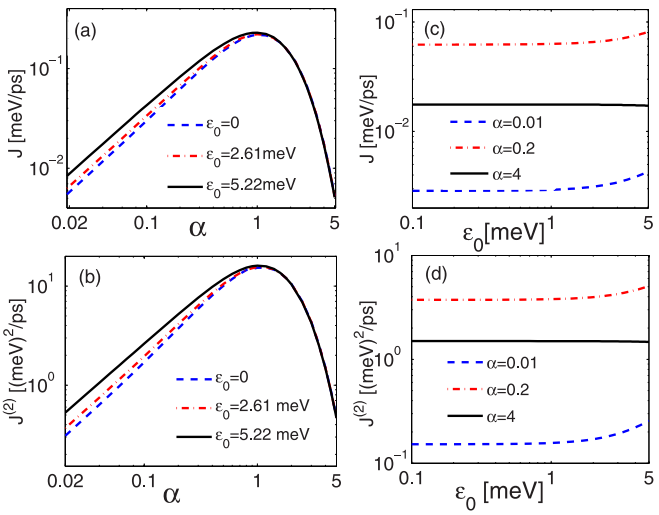

FIG. 3. Behaviors of the steady-state heat flux and noise power: (a), (b) with varying system-bath coupling strengths and (c), (d) with tuning of the qubit energy bias, respectively. Other parameters are $\Delta = 5.22$ meV, $\omega_c = 26.1$ meV, $T_L = 150$ K, and $T_R = 90$ K.

Here, we show the full counting statistics of heat transfer at steady state by analytically exhibiting the counting field based on the cumulant generating function (G_χ). Since G_χ corresponds to the ground-state energy ($E_0(\chi) = -G_\chi$), based on the analysis in Appendix A, we obtain the ground eigensolution in Liouville space as

$$E_0(\chi) = \left(X_e - X_e^\chi\right) + \frac{Y - \sqrt{Y_\chi^2 - \left(X_o^\chi\right)^2 + (X_o)^2}}{2}. \quad (20)$$

The contributing term from the even parity is

$$X_e^\chi = \Gamma_{e,+}^\chi(0) + \Gamma_{e,-}^\chi(0), \quad (21)$$

and $X_e = X_e^\chi|_{\chi=0}$, with the transition rate $\Gamma_{l,\sigma}^\chi(\omega)$ given in Eq. (16). The terms from the odd parity are given by

$$Y_\chi = \sum_{\sigma=\pm,\omega=\pm\Lambda} \Gamma_{o,\sigma}^\chi(\omega), \quad (22)$$

$$X_o^\chi = \sum_{\sigma=\pm,\omega=\pm\Lambda} \mathrm{sgn}(\omega)\sigma\Gamma_{o,\sigma}^\chi(\omega), \quad (23)$$

with $\mathrm{sgn}(\pm\Lambda) = \pm 1$ and $\Lambda = \eta\Delta$. $Y = Y_\chi|_{\chi=0}$ and $X_o = X_o^\chi|_{\chi=0}$. Consequently, the heat flux can be expressed as

$$J = \frac{\Lambda^2}{8\pi}\int_{-\infty}^{\infty}\left[\frac{\mathrm{Re}[\Gamma_o(\Lambda)]C_o(-\Lambda,\omega')+\mathrm{Re}[\Gamma_o(-\Lambda)]C_o(\Lambda,\omega')}{\mathrm{Re}[\Gamma_o(\Lambda)]+\mathrm{Re}[\Gamma_o(-\Lambda)]} + C_e(0,\omega')\right]\omega' d\omega', \quad (24)$$

where the rate probability densities are specified as

$$C_e(\omega,\omega') = \int_{-\infty}^{\infty} d\chi e^{-i\chi\omega'}\int_{-\infty}^{\infty} d\tau e^{i\omega\tau}[\cosh Q(\tau-\chi) - 1], \quad (25)$$

$$C_o(\omega,\omega') = \int_{-\infty}^{\infty} d\chi e^{-i\chi\omega'}\int_{-\infty}^{\infty} d\tau e^{i\omega\tau}\sinh Q(\tau-\chi) \quad (26)$$

at energy $\omega = 0, \pm\Lambda$. This analytical expression, Eq. (24), of the steady-state heat flux without bias is found to be identical to the counterpart in Ref. [28]; the turnover behavior of the coupling strength is exhibited in Fig. 3(a) (dashed blue line). Physically, $C_e(0,\omega')$ and $C_o(\pm\Lambda,\omega')$ describe the even- and odd-parity components of the transfer process, respectively. For example, $C_o(\Lambda,\omega')$ describes the process in which the quit releases energy Λ by relaxing from the excited eigenstate to the ground one, so that the right bath absorbs energy ω' and the left one obtains the left $\Lambda - \omega'$. As such, the number of the state change of the qubit is odd, e.g., n times excitation and $n+1$ times relaxation lead to a relaxation as the final action. And $C_e(0,\omega')$ describes the process where the qubit has an even number of virtual state changes, i.e., n times relaxation and n times excitation, so that the central qubit remains intact and undergoes no energy change. But still, the right bath absorbs energy ω' and the left bath gains $-\omega'$ (i.e., releases ω').

Similarly, the shot noise is obtained as

$$J^{(2)} = \frac{\Lambda^2}{8\pi}\left\{\int_{-\infty}^{\infty} d\omega\left[\frac{\mathrm{Re}[\Gamma_o(-\Lambda)]C_o(\Lambda,\omega)+\mathrm{Re}[\Gamma_o(\Lambda)]C_o(-\Lambda,\omega)}{\mathrm{Re}[\Gamma_o(\Lambda)]+\mathrm{Re}[\Gamma_o(-\Lambda)]} + C_e(0,\omega)\right]\omega^2 - \frac{\int_{-\infty}^{\infty} d\omega[C_o(\Lambda,\omega)-C_o(-\Lambda,\omega)]\omega}{(\mathrm{Re}[\Gamma_o(\Lambda)]+\mathrm{Re}[\Gamma_o(-\Lambda)])^3}[\mathrm{Re}[\Gamma_o(-\Lambda)]^2\int_{-\infty}^{\infty}\frac{d\omega}{\pi}C_o(\Lambda,\omega)\omega - \mathrm{Re}\left[\Gamma_o(\Lambda)^2\int_{-\infty}^{\infty}\frac{d\omega}{\pi}C_o(-\Lambda,\omega)\omega\right]\right\}. \quad (27)$$

We find that the first term on the right-hand side of Eq. (27) is the main contribution to the shot noise, of which the spectral distribution is the same as that for the heat flux in Eq. (24). Hence, the nonmonotonic turnover behavior is quite similar to the heat flux, as shown in Fig. 3(b).

2. *Biased condition:* $\epsilon_0 \neq 0$

Next, we extend our analysis of steady-state behaviors to the biased condition ($\epsilon_0 \neq 0$). The heat flux shows the same nonmonotonic turnover behavior as α increases, i.e., the flux increases in the weak and moderate coupling strength regimes ($\alpha \lesssim 1$) and decreases in the strong coupling regimes ($\alpha \gtrsim 1$), shown in Fig. 3(a). Interestingly, in the weak coupling regime ($\alpha \lesssim 1$), the heat flux is enhanced by enlarging the qubit energy bias ϵ_0, whereas as the coupling strength enters into the strong regime ($\alpha \gtrsim 1$), the heat flux remains constant for changing energy bias. To confirm these results, we select typical coupling strengths to clearly demonstrate the influence of the energy bias on the heat flux, in Fig. 3(c).

Moreover, we look into the second-cumulant heat fluctuation, i.e., the noise power, in Fig. 3(b). Similarly to the steady-state flux, the shot noise of the heat flux also exhibits the same turnover behavior. As the system-bath coupling strength increases, the noise power is enhanced by the energy bias in the weak coupling regime, whereas the noise power becomes nearly independent of the bias in the strong coupling regime. These behaviors are clearly depicted in Fig. 3(d). Therefore, we conclude that both the steady-state heat flux and the noise power are tuned in a similar way by either qubit-bath coupling or qubit energy bias.

B. Geometric-phase-induced heat flux

As the system is periodically driven by external fields, e.g., modulated by two bath temperatures $T_{L(R)}(t)$, as schematically shown in Fig. 1, the Liouville superoperator becomes time dependent $\hat{\mathcal{L}}_\chi(t)$. The effect of the geometric phase will additionally contribute to the heat flux [15,16,45–48], demonstrated in Appendix B. Thus, in the adiabatic modulation limit, there clearly exist two components making up the generating function as

$$\lim_{t\to\infty}\mathcal{Z}_\chi(t) = e^{G_\chi t} = \exp([G_{\mathrm{dyn}}(\chi) + G_{\mathrm{geom}}(\chi)]t), \quad (28)$$

Specifically, the average dynamical phase is expressed as $G_{\mathrm{dyn}}(\chi) = -\frac{1}{T_p}\int_0^{T_p} dt E_0(\chi,t)$, where T_p is the driving period, and $E_0(\chi,t)$ is the eigenvalue of $\hat{\mathcal{L}}_\chi(t)$ with the minimal real part. It results in the dynamical heat flux $J_{\mathrm{dyn}} = \frac{\partial}{\partial(i\chi)}G_{\mathrm{dyn}}(\chi)|_{\chi=0}$. The geometric phase contribution

of the generating function is described by Eq. (B9) in Appendix B,

$$G_{\rm geom}(\chi) = -\frac{1}{T_p}\int_0^{T_p} dt\langle\Phi_\chi(t)|\frac{\partial}{\partial t}|\Psi_\chi(t)\rangle, \qquad (29)$$

where $|\Psi_\chi(t)\rangle$ ($\langle\Phi_\chi(t)|$) is the corresponding right (left) eigenvector of $E_0(\chi,t)$. Assuming that the two system parameters $u_1(t)$ and $u_2(t)$ are periodically modulated [which are two driving bath temperatures $T_{L(R)}(t)$ in this work], the geometric phase in Eq. (29) is specified as $G_{\rm geom}(\chi) = -\frac{1}{T_p}\oint[du_1\langle\Phi_\chi|\frac{\partial}{\partial u_1}|\Psi_\chi\rangle + du_2\langle\Phi_\chi|\frac{\partial}{\partial u_2}|\Psi_\chi\rangle]$. According to the Stocks theorem, $G_{\rm geom}(\chi)$ can be reexpressed as

$$G_{\rm geom}(\chi) = -\frac{1}{T_p}\iint_{u_1,u_2} du_1du_2\mathcal{F}_\chi(u_1,u_2), \qquad (30)$$

where

$$\mathcal{F}_\chi(u_1,u_2) = \langle\partial_{u_1}\Phi_\chi|\partial_{u_2}\Psi_\chi\rangle - \langle\partial_{u_2}\Phi_\chi|\partial_{u_1}\Psi_\chi\rangle. \qquad (31)$$

It is noteworthy [49] that $\mathcal{F}_\chi(u_1,u_2)$ has the meaning of curvature in the parameter space (u_1,u_2) of the ground state of the quantum Liouville superoperator $\hat{\mathcal{L}}_\chi$. It is of pure geometric interpretation and independent of the driving speed (in the adiabatic limit). Mathematically, $G_{\rm geom}(\chi)$ is an analog of the adiabatic Berry phase in quantum mechanics [50], where in the latter case the wave function obtains an extra phase after a cyclic evolution. Similarly, in the full counting statistics of our driven systems, the cumulant generating function $G_{\rm geom}(\chi)$ (analog of phase) in the exponent of the characteristic function $\mathcal{Z}_\chi$ (analog of wave function) also obtains an additional term. Both extra terms share a similar geometric origin from the nontrivial curvature in the system's parameter space. As such $\mathcal{F}_\chi(u_1,u_2)$ is a Berry-like curvature and we term $G_{\rm geom}(\chi)$ the geometric phase contribution, which generates the nth cumulant of the geometric-phase-induced heat current fluctuation, as [15,16,45]

$$J^{(n)}_{\rm geom} = \frac{\partial^n G_{\rm geom}(\chi)}{\partial(i\chi)^n}\bigg|_{\chi=0} = -\frac{1}{T_p}\iint_{u_1,u_2} du_1du_2\frac{\partial^n}{\partial(i\chi)^n}\mathcal{F}_\chi(u_1,u_2)|_{\chi=0}. \qquad (32)$$

The geometric heat flux is given by the first cumulant $J_{\rm geom} = J^{(1)}_{\rm geom}$.

1. *Unbiased condition:* $\epsilon_0 = 0$

Here, we first investigate the geometric heat flux without bias ($\epsilon_0 = 0$). It is known that in the weak qubit-bath coupling regime, the geometric-phase-induced heat flux is finite and independent of the coupling strength [15]. This mainly results from the fact that with weak qubit-bath coupling the transition rates between the two-level qubit and the phononic baths are linearly dependent on the coupling strength, exhibiting additive transfer processes. On the contrary, the geometric heat flux vanishes in the strong qubit-bath coupling regime upon applying the nonequilibrium NIBA method [16]. The left and right eigenvectors corresponding to the ground-state energy are given by $|\Psi_\chi\rangle = \frac{1}{2}[1,1,0,0]^T$ and $\langle\Phi_\chi| = [1,1,0,0]$, which are clearly independent of the system parameters and result in the zero geometric heat flux according to Eq. (30). It was proposed

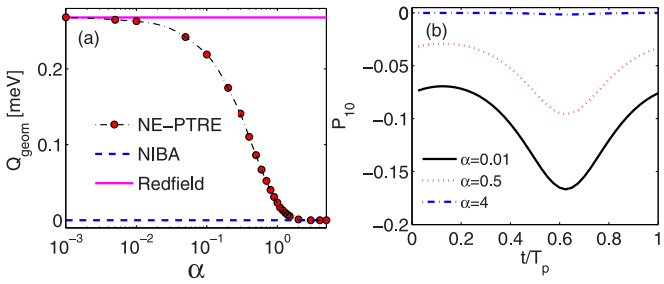

FIG. 4. Adiabatic modulation by two bath temperatures without bias ($\epsilon_0 = 0$): (a) geometric-phase-induced heat pump $Q_{\rm geom} = J_{\rm geom} * T_p$; (b) coherence ($P_{10}$) in the local basis. The two bath temperatures are specified as $T_L(\tau) = (150 + 90\cos\Omega_p\tau)$ K and $T_R(\tau) = (150 + 90\sin\Omega_p\tau)$ K, with the period $T_p = 1$ ns. Other parameters are $\Delta = 5.22$ meV and $\omega_c = 26.1$ meV.

that these two approaches describe different physical pictures within the same NESB system and do not conflict with each other [16,28].

Based on the χ-dependent NE-PTRE, Eq. (16), we try to explicitly unify these limiting results, as shown in Fig. 4(a). In the weak system-bath coupling regime, the geometric heat flux approaches the upper limit within the Redfield scheme. As the coupling strength increases, the geometric heat flux is strongly suppressed and asymptotically decreases to 0, which finally becomes identical to the result in the nonequilibrium NIBA. The underlying mechanism can be understood by analyzing the coherence $P_{10}(t)$, since the populations (P_{00}, P_{11}) are constant. We find in Fig. 4(b) that the coherence is suppressed monotonically by increasing the qubit-bath coupling strength, finally resulting in the constant quasi–steady state in the strong coupling limit [16]. It is proposed that without bias ($\epsilon_0 = 0$), multiphonon processes degrade the formation of the geometric phase. Therefore, this seeming contradiction is clearly solved within the framework of the NE-PTRE accompanied by a counting field.

Moreover, compared to the dynamical heat flux [28], the system-bath coupling plays a distinct role in the geometric heat flux. For the dynamical flux, in the weak and intermediate coupling regimes, multiphonon processes are helpful in generating steady-state heat flux, mainly due to the robustness of the transition rates. However, in the strong coupling limit, the large system-bath interaction weakens the transition rates due to the quantum Zeno-like effect and, finally, suppresses the heat flux. Hence, the nonmonotonic behavior of the dynamical heat flux is clearly demonstrated. For geometric flux, increasing the system-bath coupling strength will only monotonically decrease the geometric heat flux, which implies that the instantaneous state of the qubit is inclined to remain intact, which is independent of temperature modulations, as we have discussed above.

2. *Biased condition:* $\epsilon_0 \neq 0$

Next, we analyze the geometric heat flux under finite energy bias ($\epsilon_0 \neq 0$), as shown in Fig. 5(a). In the weak coupling limit, the geometric heat flux is equal to that from the Redfield scheme. The existence of coherence P_{10} is also crucial to enhance the geometric-phase-induced heat flux, which is similar to the unbiased case in Fig. 4. As the coupling strength

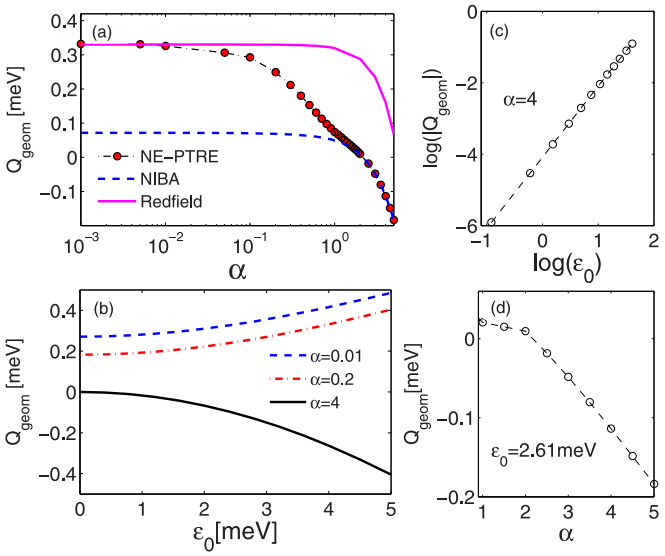

FIG. 5. (a) Geometric-phase-induced heat pump $Q_{\rm geom} = J_{\rm geom} \times T_p$ under finite energy bias of the qubit ($\epsilon_0 = 2.61$ meV); (b) influence of the qubit energy bias on the geometric-phase-induced heat pump, with modulation of the two bath temperatures; (c) log-log relation between ϵ_0 and $Q_{\rm geom}$ in the strong coupling regime ($\alpha = 4$); (d) linear relation between $Q_{\rm geom}$ and α in the strong coupling regime. Parameters are the same as in Fig. 4.

increases, the geometric heat flux decreases sharply and even becomes negative. The corresponding coherence is strongly suppressed, which leaves only the populations to contribute to the geometric heat flux. Then the behavior of the geometric heat flux is consistent with the result within the nonequilibrium NIBA in the strong coupling regime [16]. As a result, we conclude that the NE-PTRE is also applicable to unify limiting coupling results beyond the unbiased condition.

Next, we turn to analyze the influence of the qubit energy bias on the geometric heat pump in Fig. 5(b). In the weak qubit-bath coupling regime (e.g., $\alpha = 0.01$), the geometric heat pump shows monotonic enhancement with an increase in the energy bias. As the interaction strength is modulated to the intermediate coupling regime (e.g., $\alpha = 0.2$), the geometric heat pump is also positively enhanced by the increasing energy bias, which is similar to the counterpart in the weak coupling case. If we further increase the coupling strength (e.g., $\alpha = 4$), the geometric heat pump becomes negatively enhanced, which is quantitatively distinct from that in the weak coupling regime. This observation clearly demonstrates different physical pictures in these two limiting interaction regimes.

We admit that it is beyond our ability to analytically provide a comprehensive picture in a wide system-bath coupling regime for the biased case. Here, to understand the geometric heat flux reversal, we focus on the strong interaction limit, which is consistent with the nonequilibrium NIBA framework. Combined with the counting filed, the equation of motion for the qubit is expressed as

$$\frac{d}{dt}\begin{pmatrix} P_{11}^{\chi} \\ P_{00}^{\chi} \end{pmatrix} = -\begin{pmatrix} K(\epsilon_0) & -K_-(\chi) \\ -K_+(\chi) & K(-\epsilon_0) \end{pmatrix}\begin{pmatrix} P_{11}^{\chi} \\ P_{00}^{\chi} \end{pmatrix}, \tag{33}$$

with the population $P_{ii}^{\chi} = \langle i|\hat{\rho}_{\chi}(t)|i\rangle$. The transition rates are given by

$$K^{\pm}(\chi) = (\Delta/2)^2 \int_{-\infty}^{\infty} dt \eta^2 e^{\pm i\epsilon_0 t + Q_L(t) + Q_R(t-\chi)}, \tag{34}$$

with $K(\pm\epsilon_0) = K_{\pm}(\chi)|_{\chi=0}$, η and $Q_v(t)$ given in Eq. (3) and Eq. (8), respectively. Thus, the eigenstate energies are directly obtained as

$$E_{\pm}(\chi) = \tfrac{1}{2}\{[K(\epsilon_0) + K(-\epsilon_0)] \pm \sqrt{[K(\epsilon_0) - K(-\epsilon_0)]^2 + 4K_+(\chi)K_-(\chi)}\}. \tag{35}$$

The corresponding right eigenstates are given by

$$|\Psi_{\chi}^{\pm}\rangle = [2K_-(\chi), A_{\pm}(\chi)]^T, \tag{36}$$

with the coefficients $A_{\pm}(\chi) = [K(\epsilon_0) - K(-\epsilon_0)] \mp \sqrt{[K(\epsilon_0) - K(-\epsilon_0)]^2 + 4K_+(\chi)K_-(\chi)}$. Accordingly, the left eigenstates are

$$\langle\Phi_{\chi}^{\pm}| = \frac{[2K_+(\chi), A_{\pm}(\chi)]}{A_{\pm}^2(\chi) + 4K_+(\chi)K_-(\chi)}. \tag{37}$$

In the strong qubit-bath coupling limit, it is known that the Marcus approximation becomes applicable [9,51]. Marcus's theory was originally proposed for the electron transfer rate in the donor-acceptor species. And it works at high temperatures $k_B T > \epsilon_0$ and/or the strong qubit-bath coupling regime [52]. It can be approached by the short-time expansion of $Q_v(t)$ in Eq. (8) as $Q_v(t) = \frac{\Gamma_v T_v}{\omega_{c,v}^2} - \Gamma_v T_v t^2 - i\Gamma_v t$ [54], with the effective coupling strength $\Gamma_v = \int \frac{J_v(\omega)}{\pi\omega} d\omega = 2\alpha_v \omega_{c,v}$. Consequently, the transition rates combined with the counting parameter are simplified as $K_{\pm}(\chi) = K(\pm\epsilon_0)M_{\pm}(\chi)$, with the standard rates

$$K(\pm\epsilon_0) = \frac{\Delta^2}{4}\sqrt{\frac{\pi}{\Gamma_L T_L + \Gamma_R T_R}} \exp\left[-\frac{(\epsilon_0 \mp \Gamma_L \mp \Gamma_R)^2}{4(\Gamma_L T_L + \Gamma_R T_R)}\right] \tag{38}$$

and the factor

$$M_{\pm}(\chi) = e^{\pm i\epsilon_0\chi - \frac{\Gamma_L T_L \Gamma_R T_R}{\Gamma_L T_L + \Gamma_R T_R}[i\chi(\frac{1}{T_L} + \frac{\pm\epsilon_0 - \Gamma_R}{\Gamma_R T_R}) + \chi^2]}. \tag{39}$$

In the absence of the counting field ($\chi = 0$), the factor $M_{\pm}(\chi = 0) = 1$, and the modified transition rates $K_{\pm}(\chi)$ decrease back to the standard expressions $K(\pm\epsilon_0)$ in Eq. (38), respectively. Moreover, we consider the weak qubit energy bias regime, i.e., $\epsilon_0 \ll \{\Gamma_v, k_B T_v\}$. Then the transition rate in Eq. (38) can be approximately expanded up to first order of ϵ_0 as

$$K(\pm\epsilon_0) \approx K_0\left[1 \pm \frac{\epsilon_0}{2(\Gamma_L T_L + \Gamma_R T_R)}(\Gamma_L + \Gamma_R)\right], \tag{40}$$

with $K_0 = \frac{\Delta^2}{4}\sqrt{\frac{\pi}{\Gamma_L T_L + \Gamma_R T_R}} \exp[-\frac{(\Gamma_L + \Gamma_R)^2}{4(\Gamma_L T_L + \Gamma_R T_R)}]$. According to the definition in Eq. (32), the geometric-phase-induced heat flux is obtained as

$$J_{\rm geom} = -\frac{\epsilon_0^2}{T_p} \iint_{T_L, T_R} dT_L dT_R \frac{\Gamma_L \Gamma_R (\Gamma_L + \Gamma_R)^3}{8(\Gamma_L T_L + \Gamma_R T_R)^4}. \tag{41}$$

This expression clearly confirms the reversal (negative) behavior of the heat flux in the strong coupling limit, shown in Fig. 5(a). Moreover, the power-law feature of the energy bias

is analytically exhibited in Eq. (41), which is in excellent agreement with the numerical result as $J_{\rm geom}\sim-\epsilon_0^{2.0\pm0.02}$, shown in Fig. 5(c). If the system-bath couplings are identically selected as $\alpha_L=\alpha_R=\alpha$, the geometric heat flux is expressed as $J_{\rm geom}\sim-\alpha\epsilon_0^2$ based on Eq. (41), and numerically confirmed in Fig. 5(d), which coincides with the numerical results in Fig. 2 of Ref. [16], that $J_{\rm geom}$ is linearly dependent on the coupling strength α and quadratically dependent on the qubit energy bias ϵ_0.

V. CONCLUSION

In summary, we have investigated the geometric-phase-induced heat pump in the nonequilibrium spin-boson model by periodically modulating the temperatures of two thermal baths, which is beyond the traditional Redfield and nonequilibrium NIBA schemes. With the development of the nonequilibrium polaron-transformed Redfield equation (NE-PTRE) approach in the context of full counting statistics, the cumulant generating function is clearly demonstrated; it consists of both dynamical phase and geometric phase contributions. In the absence of an external driving field, the influences of qubit energy bias on the steady-state heat flux and the corresponding noise power have been analyzed. In the weak and moderate coupling regimes, the energy bias monotonically enhances both the steady state heat flux and the noise power, while in the strong coupling regime, these two observables become independent of the energy bias. This clearly demonstrates the same role of the energy bias in affecting the heat flux and the noise power.

Next, we have analyzed the geometric heat pump without bias by varying the qubit-bath coupling strength over a wide regime. In the weak system-bath coupling limit, the geometric heat flux is positive finite, which is equivalent to the counterpart within the Redfield scheme [15]. As the coupling strength increases, the geometric heat flux shows a monotonic decrease and, finally, approaches strictly 0, which is identical to the result based on the nonequilibrium NIBA [16]. We have also studied the geometric heat pump under the biased condition. We found that the geometric heat pump decreases quickly as the qubit-bath coupling increases and shows reversal behavior in the strong coupling regime. Moreover, the analytical relations of the geometric heat flux with the system-bath coupling and the energy bias have been obtained. The results based on the NE-PTRE also show consistency with the counterparts from the Redfield and nonequilibrium NIBA schemes, in the weak and strong coupling regimes, respectively.

Therefore, we conclude that this unified theory is applicable to obtain the geometric heat flux in the nonequilibrium spin-boson model, under both unbiased and biased conditions. Moreover, we have analyzed the influence of the qubit energy bias on the geometric heat pump. The geometric heat flux is negatively enhanced in the strong qubit-bath coupling regime, which is in sharp contrast with its counterpart in the weak coupling case, exhibiting positive stabilization. We hope that these results will have broad implications for smart control of energy transfer in low-dimensional nanodevices.

ACKNOWLEDGMENTS

C.W. is supported by the National Natural Science Foundation of China under Grants No. 11547124 and No. 11574052. J.R. acknowledges the National Youth 1000 Talents Program in China and the 985 startup grant (No. 205020516074) at Tongji University.

APPENDIX A: ANALYTICAL EXPRESSION OF THE STEADY-STATE CUMULANT GENERATING FUNCTION WITHOUT BIAS

Without bias ($\epsilon_0=0$), the Liouvillian dynamics of the reduced density matrix in Eq. (19) under the framework of full counting statistics is expressed as $\frac{d}{dt}|\rho_\chi\rangle=-\hat{L}_\chi|\rho_\chi\rangle$, where the evolution matrix is specified as

$$\hat{L}_\chi=\begin{pmatrix} a & -a_\chi & b_\chi & c_\chi \\ -a_\chi & a & c_\chi & b_\chi \\ d_\chi & e_\chi & a & f_\chi \\ e_\chi & d_\chi & f_\chi & a \end{pmatrix}. \tag{A1}$$

The matrix elements are written as $a_\chi=X_e^\chi+\frac{Y_\chi}{2}$, $b_\chi=-\frac{1}{2}(X_{o,+}^\chi+X_{o,-})$, $c_\chi=\frac{1}{2}(X_{o,+}+X_{o,-}^\chi)$, $d_\chi=\frac{1}{2}(X_{o,+}^\chi-X_{o,-})$, $e_\chi=\frac{1}{2}(X_{o,+}-X_{o,-}^\chi)$, $f_\chi=-X_e^\chi+\frac{Y_\chi}{2}$, and $a=a_\chi|_{\chi=0}$, with the coefficients

$$X_e^\chi=\Gamma_{e,+}^\chi(0)+\Gamma_{e,-}^\chi(0), \tag{A2}$$

$$Y_\chi=\Gamma_{o,+}^\chi(\Lambda)+\Gamma_{o,+}^\chi(-\Lambda)+\Gamma_{o,-}^\chi(\Lambda)+\Gamma_{o,-}^\chi(-\Lambda), \tag{A3}$$

$$X_{o,\pm}^\chi=\Gamma_{o,\pm}^\chi(\Lambda)-\Gamma_{o,\pm}^\chi(-\Lambda), \tag{A4}$$

and $X_{o,\pm}=X_{o,\pm}^\chi|_{\chi=0}$. The modified transition rates $\Gamma_{e(o)}^\chi(\omega)$ are shown in Eq. (16).

To find the eigenvalues of the evolution matrix, we set $\det(\mathrm{L}_\chi-\lambda\mathrm{I})=0$, which results in

$$\begin{aligned}(a-\lambda)^2=&(a_\chi f_\chi+b_\chi d_\chi+c_\chi e_\chi)\\&\pm[(a_\chi-f_\chi)(a-\lambda)+(c_\chi d_\chi+b_\chi e_\chi)].\end{aligned} \tag{A5}$$

For one branch, the solution is given by

$$\begin{aligned}\lambda_\pm^p=&\left(X_e-X_e^\chi\right)+\frac{Y}{2}\\&\mp\sqrt{Y_\chi^2-\left(X_{o,+}^\chi-X_{o,-}^\chi\right)^2+(X_{o,+}-X_{o,-})^2}/2,\end{aligned} \tag{A6}$$

and for the other branch, it is given by

$$\begin{aligned}\lambda_\pm^m=&\left(X_e+X_e^\chi\right)+\frac{Y}{2}\\&\mp\sqrt{Y_\chi^2-\left(X_{o,+}^\chi+X_{o,-}^\chi\right)^2+(X_{o,+}+X_{o,-})^2}/2.\end{aligned} \tag{A7}$$

Hence, the ground-state energy is obtained as $E_0(\chi)=\lambda_+^p$. Since the cumulant generating function is given by $G_\chi=-E_0(\chi)$, it is specified as

$$G_\chi=\left(X_e^\chi-X_e\right)-\frac{Y}{2}+\sqrt{Y_\chi^2-(X_o^\chi)^2+(X_o)^2}/2, \tag{A8}$$

with $X_o^\chi=X_{o,+}^\chi-X_{o,-}^\chi$ and $X_o=X_o^\chi|_{\chi=0}$.

APPENDIX B: INTRODUCTION OF THE GEOMETRIC PHASE AND CUMULANT GENERATING FUNCTION

Considering the time-dependent superoperator $\hat{L}_\chi(t)$ with the counting parameter, which is not Hermitian, we obtain the quasi-eigensolution as

$$\begin{aligned}\hat{L}_\chi(t)|\psi_n(\chi,t)\rangle &= E_n(\chi,t)|\psi_n(\chi,t)\rangle,\\ \langle\phi_n(\chi,t)|\hat{L}_\chi(t) &= \langle\phi_n(\chi,t)|E_n(\chi,t),\end{aligned} \tag{B1}$$

where $\lambda_n(\chi,t)$ is the instantaneous eigenvalue of $\hat{L}_\chi(t)$, and $|\psi_n(\chi,t)\rangle$ ($\langle\phi_n(\chi,t)|$) is the corresponding normalized right (left) eigenvector, which obeys the relation $\langle\phi_n(\chi,t)|\psi_n(\chi,t)\rangle = \delta_{n,m}$. In analogy with the seminal Berry's solution, we can express the wave function in the basis $\{|\psi_n(\chi,t)\}$ as

$$|\rho_\chi(t)\rangle = \sum_n a_n(t)\exp\left[-\int_0^t E_n(\chi,\tau)d\tau\right]|\psi_n(\chi,t)\rangle. \tag{B2}$$

By substituting Eq. (B2) into the dynamical equation, (19), we obtain the evolution equation of $a_n(t)$:

$$\begin{aligned}&\sum_n \frac{da_n(t)}{dt}\exp\left[-\int_0^t E_n(\chi,\tau)d\tau\right]|\psi_n(\chi,t)\rangle\\ &= -\sum_n a_n(t)\exp\left[-\int_0^t E_n(\chi,\tau)d\tau\right]\left|\frac{d}{dt}\psi_n(\chi,t)\right\rangle.\end{aligned} \tag{B3}$$

Then, by left-multiplying the eigenvector $\langle\phi_m(\chi,t)|$ by Eq. (B3), we find that

$$\begin{aligned}\frac{da_m(t)}{dt} &= -a_m(t)\left\langle\phi_m(\chi,t)\left|\frac{d}{dt}\psi_m(\chi,t)\right\rangle\right.\\ &\quad-\sum_{n\neq m}a_n(t)\exp\left(-\int_0^t[E_n(\chi,\tau)-E_m(\chi,\tau)]d\tau\right)\\ &\quad\times\left\langle\phi_m(\chi,t)\left|\frac{d}{dt}\psi_n(\chi,t)\right\rangle\right..\end{aligned} \tag{B4}$$

It should be noted that the eigenvalue $E_n(\chi,t)$ generally is a complex value. Hence, the long-time behavior of the reduced qubit system is mastered by only the eigenmode $m = 0$, of which the eigenvalue $E_0(\chi,t)$ owns the smallest real part.

In the adiabatic limit, the second term on the right-hand side of Eq. (B4) can be approximately ignored due to the decay factor $\exp(-\int_0^t[E_n(\chi,\tau)-E_0(\chi,\tau)]d\tau)$ ($\mathrm{Re}[E_n(\chi,\tau)-E_0(\chi,\tau)] > 0$ for $n\neq 0$). We obtain the expression of $a_n(t)$ after long-time evolution ($t\to\infty$) as

$$a_0(t) = \exp\left(-\int_0^t\left\langle\phi_0(\chi,\tau)\left|\frac{d}{d\tau}\psi_0(\chi,\tau)\right\rangle\right.d\tau\right)a_0(0), \tag{B5}$$

with $a_0(0)$ the initial-state coefficient. Then, if we consider the adiabatic cyclic evolution over a long time period T_p, the wave function can be specified as

$$\begin{aligned}|\rho_\chi(t)\rangle = \exp\Bigg(&-\frac{t}{T_p}\int_0^{T_p}d\tau\Bigg[E_0(\chi,\tau)\\ &+\left\langle\phi_0(\chi,\tau)\left|\frac{d}{d\tau}\psi_0(\chi,\tau)\right\rangle\right.\Bigg]\Bigg)a_0(0)|\rho_\chi(0)\rangle.\end{aligned} \tag{B6}$$

Consequently, the generating function can be obtained as

$$\begin{aligned}\mathcal{Z}_\chi(t) &= \langle \mathrm{I}|\rho_\chi(t)\rangle\\ &\approx\exp\Bigg(-\frac{t}{T_p}\int_0^{T_p}d\tau\Bigg[E_0(\chi,\tau)\\ &\quad+\left\langle\phi_0(\chi,\tau)\left|\frac{d}{d\tau}\psi_0(\chi,\tau)\right\rangle\right.\Bigg]\Bigg)a_0(0)\langle\mathrm{I}|\rho_\chi(0)\rangle.\end{aligned} \tag{B7}$$

Finally, the cumulant generating function in the long-time limit can be described by two contributing terms as

$$G(\chi) = \lim_{t\to\infty}\frac{\ln\mathcal{Z}_\chi(t)}{t} = G_{\mathrm{dyn}}(\chi) + G_{\mathrm{geom}}(\chi), \tag{B8}$$

and the factor $\lim_{t\to\infty}\frac{1}{t}\ln(a_0(0)\langle\mathrm{I}|\rho_\chi(0)\rangle)$ becomes negligible. Here, $G_{\mathrm{dyn}}(\chi)$ is the dynamical phase factor, written as $G_{\mathrm{dyn}}(\chi) = -\frac{1}{T_p}\int_0^{T_p}E_0(\chi,\tau)d\tau$, while $G_{\mathrm{dyn}}(\chi)$ originates from the geometric phase contribution, written as $G_{\mathrm{geom}}(\chi) = -\frac{1}{T_p}\int_0^{T_p}\langle\phi_0(\chi,\tau)|\frac{d}{d\tau}\psi_0(\chi,\tau)\rangle d\tau$. In the text, we use $|\Psi_\chi(t)\rangle\langle\langle\Phi_\chi(t)|)$ in Eq. (29) to replace $|\psi_0(\chi,t)\rangle\langle\langle\phi_0(\chi,t)|)$. The geometric-phase-induced cumulant generating function is reexpressed as

$$G_{\mathrm{geom}}(\chi) = -\frac{1}{T_p}\int_0^{T_p}\left\langle\Phi_\chi(\tau)\left|\frac{d}{d\tau}\Psi_\chi(\tau)\right\rangle\right.d\tau. \tag{B9}$$

[1] Y. Dubi and M. Di Ventra, Rev. Mod. Phys. **83**, 131 (2011).
[2] M. A. Ratner, Nat. Nanotechnol. **8**, 378 (2013).
[3] P. Nalbach and M. Thorwart, Proc. Natl. Acad. Sci. USA **110**, 2693 (2013).
[4] M. Mohseni, Y. Omar, G. S. Engel, and M. B. Plenio, *Quantum Effects in Biology* (Cambridge University Press, Cambridge, UK, 2014).
[5] D. Z. Xu and J. S. Cao, Front. Phys. **11**, 110308 (2016).
[6] N. B. Li, J. Ren, L. Wang, G. Zhang, P. Hänggi, and B. W. Li, Rev. Mod. Phys. **84**, 1045 (2012).
[7] J. Ren and B. W. Li, AIP Adv. **5**, 053101 (2015).
[8] D. Segal and A. Nitzan, Phys. Rev. Lett. **94**, 034301 (2005).
[9] D. Segal, Phys. Rev. B **73**, 205415 (2006).
[10] C. W. Chang, D. Okawa, A. Majumdar, and A. Zettl, Science **314**, 1121 (2006).
[11] L. Wang and B. W. Li, Phys. Rev. Lett. **99**, 177208 (2007).
[12] L. F. Zhang, J. Ren, J. S. Wang, and B. W. Li, Phys. Rev. Lett. **105**, 225901 (2010).
[13] E. Taylor and D. Segal, Phys. Rev. Lett. **114**, 220401 (2015).
[14] D. Segal, Phys. Rev. Lett. **101**, 260601 (2008).
[15] J. Ren, P. Hanggi, and B. W. Li, Phys. Rev. Lett. **104**, 170601 (2010).
[16] T. Chen, X. B. Wang, and Jie Ren, Phys. Rev. B **87**, 144303 (2013).
[17] C. Uchiyama, Phys. Rev. E **89**, 052108 (2014).
[18] K. Saito and T. Kato, Phys. Rev. Lett. **111**, 214301 (2013).
[19] A. J. Leggett, S. Chakravarty, A. T. Dorsey, M. P. A. Fisher, A. Garg, and W. Zwerger, Rev. Mod. Phys. **59**, 1 (1987).
[20] U. Weiss, *Quantum Dissipative Systems* (World Scientific, Singapore, 2008).
[21] L. Nicolin and D. Segal, J. Chem. Phys. **135**, 164106 (2011).
[22] L. Nicolin and D. Segal, Phys. Rev. B **84**, 161414 (2011).

[23] D. Segal, Phys. Rev. E **90**, 012148 (2014).
[24] L. A. Velizhanin, H. Wang, and M. Thoss, Chem. Phys. Lett. **460**, 325 (2008).
[25] J. J. Liu, H. Xu, and C. Q. Wu, Chem. Phys. **481**, 42 (2016).
[26] J. J. Liu, H. Xu, B. W. Li, and C. Q. Wu, arXiv:1609.05598.
[27] B. K. Agarwalla and D. Segal, arXiv:1612.01008.
[28] C. Wang, J. Ren, and J. S. Cao, Sci. Rep. **5**, 11787 (2015).
[29] S. Gasparinetti, P. Solinas, A. Braggio, and M. Sassetti, New J. Phys. **16**, 115001 (2014).
[30] G. Guarnieri, C. Uchiyama, and B. Vacchini, Phys. Rev. A **93**, 012118 (2016).
[31] J. Cerrillo, M. Buser, and T. Brandes, Phys. Rev. B **94**, 214308 (2016).
[32] M. Carrega, P. Solinas, M. Sassetti, and U. Weiss, Phys. Rev. Lett. **116**, 240403 (2016).
[33] L. Ferialdi, Phys. Rev. A **95**, 020101(R) (2017).
[34] D. J. Thouless, Phys. Rev. B **27**, 6083 (1983).
[35] A. Nazir, Phys. Rev. Lett. **103**, 146404 (2009).
[36] S. Jang, Y. C. Cheng, D. R. Reichman, and J. D. Eaves, J. Chem. Phys. **129**, 101104 (2008).
[37] P. Nalbach, J. Eckel, and M. Thorwart, New J. Phys. **12**, 065043 (2010).
[38] C. K. Lee, J. M. Moix, and J. S. Cao, J. Chem. Phys. **142**, 164103 (2015).
[39] D. Z. Xu, C. Wang, Y. Zhao, and J. S. Cao, New J. Phys. **18**, 023003 (2016).
[40] R. J. Silbey and T. Harris, J. Chem. Phys. **80**, 2615 (1984).
[41] In the eigenbasis $\{|\pm\rangle\}$ with $\hat{H}_s|\pm\rangle = \pm\Lambda/2|\pm\rangle$, the transition projectors are given by $\hat{P}_e(\Lambda) = \cos\theta|+\rangle\langle -|$, $\hat{P}_e(0) = \sin\theta(|+\rangle\langle +| - |-\rangle\langle -|)$, $\hat{P}_e(-\Lambda) = \cos\theta|-\rangle\langle +|$, $\hat{P}_o(\Lambda) = -i|+\rangle\langle -|$, $\hat{P}_o(0) = 0$, and $\hat{P}_o(-\Lambda) = i|-\rangle\langle +|$, with $\theta = \tan^{-1}(\eta\Delta/\epsilon_0)$.
[42] T. Ruokola and T. Ojanen, Phys. Rev. B **83**, 045417 (2011).
[43] M. Esposito, U. Harbola, and S. Mukamel, Rev. Mod. Phys. **81**, 1665 (2009).
[44] M. Campisi, P. Hanggi, and P. Talkner, Rev. Mod. Phys. **83**, 771 (2011).
[45] N. A. Sinitsyn and I. Nemenman, Europhys. Lett. **77**, 58001 (2007).
[46] N. A. Sinitsyn and I. Nemenman, Phys. Rev. Lett. **99**, 220408 (2007).
[47] T. Sagawa and H. Hayakawa, Phys. Rev. E **84**, 051110 (2011).
[48] T. Yuge, T. Sagawa, A. Sugita, and H. Hayakawa, Phys. Rev. B **86**, 235308 (2012).
[49] J. Ren, S. Liu, and B. Li, Phys. Rev. Lett. **108**, 210603 (2012).
[50] M. V. Berry, Proc. R. Soc. London A **392**, 45 (1984).
[51] R. A. Marcus, J. Chem. Phys. **24**, 966 (1956).
[52] We note that the Marcus theory not only is valid in the high-temperature (classic) limit $k_BT > \omega_c$, but also is valid in the relative "high" -temperature regime $\omega_c > k_BT > \epsilon_0$ (high compared to the qubit's energy scale). Under the latter regime, both the thermal fluctuation ($-\Gamma_v T_v t^2$) and the quantum dissipation ($-i\Gamma_v t$) terms of the correlation function $Q_v(t)$ coexist, which forms the basis of our discussion. Therefore, the Marcus theory can be carried out in this whole regime "$k_BT > \epsilon_0$" in our work. Related discussions can also be found preceding Eq. (37) in Ref. [21], following Eq. (18) in Ref. [22], and in subsection 5.2 in Ref. [53].
[53] L. A. Pachón and P. Brumer, Phys. Chem. Chem. Phys. **14**, 10094 (2012).
[54] Please note here that $Q_v(t)$ is different from the expression used in Ref. [16] and in Ref. [9]. This is caused by the renormalization factor η we extracted. They are consistent when we consider η.